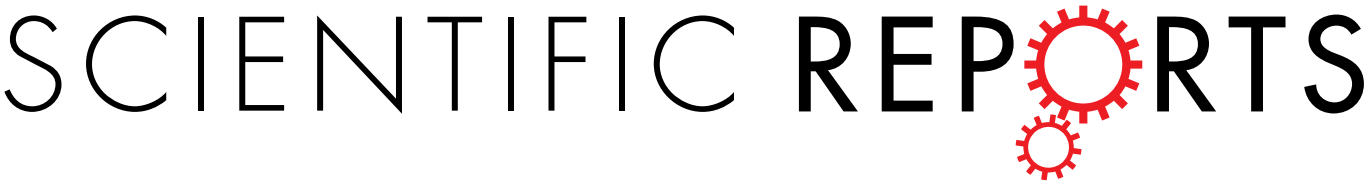

OPEN

Using non-Markovian measures to evaluate quantum master equations for photosynthesis

Received: 27 March 2015
Accepted: 09 July 2015
Published: 04 August 2015

Hong-Bin Chen[1], Neill Lambert[2], Yuan-Chung Cheng[3], Yueh-Nan Chen[1] & Franco Nori[2,4]

When dealing with system-reservoir interactions in an open quantum system, such as a photosynthetic light-harvesting complex, approximations are usually made to obtain the dynamics of the system. One question immediately arises: how good are these approximations, and in what ways can we evaluate them? Here, we propose to use entanglement and a measure of non-Markovianity as benchmarks for the deviation of approximate methods from exact results. We apply two frequently-used perturbative but non-Markovian approximations to a photosynthetic dimer model and compare their results with that of the numerically-exact hierarchy equation of motion (HEOM). This enables us to explore both entanglement and non-Markovianity measures as means to reveal how the approximations either overestimate or underestimate memory effects and quantum coherence. In addition, we show that both the approximate and exact results suggest that non-Markonivity can, counter-intuitively, increase with temperature, and with the coupling to the environment.

Modelling and understanding the non-equilibrium dynamics of open quantum systems is a ubiquitous problem in physics, chemistry and biology[1–9]. In such systems, the environment is usually composed of a huge number of microscopic constituents, an exact description of which is challenging. One can invoke intensive computational techniques, such as path-integral formalisms[1,2,10,11], Monte Carlo algorithms[12], the hierarchy equations of motion (HEOM)[13–16], the reaction-coordinate method[17,18] and others, to explicitly and exactly propagate the quantum state of a complete system-environment model. However, a common drawback of these exact numerical solutions is their demanding computational resource requirements, which can scale badly depending on the spectral density of the environment being modelled, the number of independent baths the system is coupled to, or the complexity of the system itself.

To simplify the problem and gain useful physical insights, approximations are usually made to reduce the system dynamics to that of a relatively few degrees of freedom. In that regard, much effort has been devoted to develop quantum master equations (QMEs) which describe these reduced degrees of freedom in various limits. Redfield theory[19] provides one with QME based on (together with a secular approximation) a second-order perturbation approximation in the system-environment coupling. For the strong-coupling limit, Förster theory[20–22] adopts a diffusion-rate equation[23] to describe the incoherent transport phenomenon. Nevertheless, these conventional Markovian QME treatments cannot capture the memory effects of the bath.

In order to take into account the memory effects, many attempts at improving these Markovian QMEs have been made. The second-order time-convolution (TC2)[24] equation is known as a chronological-ordering prescription[25] or time-nonlocal equation[26,27]. It is a direct generalization of Redfield QME without performing the Markov and secular approximations. The second-order time-local (TL2) equation is another frequently used QME, sometimes called a partial-time-ordering prescription[25]

[1]Department of Physics and National Center for Theoretical Sciences, National Cheng Kung University, Tainan 701, Taiwan. [2]CEMS, RIKEN, Wako-shi, Saitama 351-0198, Japan. [3]Department of Chemistry and Center for Quantum Science and Engineering, National Taiwan University, Taipei 106, Taiwan. [4]Physics Department, University of Michigan, Ann Arbor, Michigan 48109-1040, USA. Correspondence and requests for materials should be addressed to Y.-C.C. (email: yuanchung@ntu.edu.tw) or Y.-N.C. (email: yuehnan@mail.ncku.edu.tw)

or time-convolutionless equation. Some works suggest that TL2 shows better performance than TC2 at numerically approximating exact results[28]. Nevertheless, their respective domains of applicability have not been thoroughly investigated yet.

In each QME model (TC2, TL2), certain approximations and simplifications are introduced to obtain solvable equations. To investigate the deviation of each approximate QME model from the exact results, we first compare the explicit dynamics of these two approximative QMEs with that of the HEOM. The HEOM approach is considered to be numerically exact for the models with the Drude-Lorentz spectral density function investigated here. For more general bath models and dynamics at low temperatures, the need to truncate at a certain level of the hierarchy equations can lead to errors, and thus the exactness of the HEOM approach requires further scrutiny in such cases[29–31]. We focus on the intermediate system-environment coupling regime, which has proven to be the most challenging and relevant to the dynamics in realistic systems such as the photosynthetic Fenna-Matthews-Olson complex. Notably, the intermediate regime is also the one at which the region of validity of most approximations breaks down. Both approximate methods are perturbative in the system-bath coupling, but can in principle harbor memory effects of the environment.

Recently, much effort has been devoted to the quantification of memory effects[32–35] which has subsequently been studied in the context of various physical systems[36–38]. To investigate how well the models we study here capture the memory effect, we utilize the concept of the Choi-Jamiołkowski isomorphism[39,40] to encode complete information on the dynamics of the system into the entanglement with an ancilla. By comparing the time evolution of the entanglement between system and ancilla, and an associated measure of non-Markovianity[33], one can find out to what extent the memory effects and coherence predicted by each approximate QME deviates from being numerically exact. Our results suggest that entanglement and non-Markovianity provide a useful benchmark for the performance of such approximative treatments, providing a more fine-grained insight into the deviation from exact results than quantities like the fidelity alone.

In performing this analysis we also discuss several interesting physical trends, including a counter-intuitive increase of non-Markovianity with both temperature and with the coupling strength to the environment. We attribute this increase to an enhancement of system-environment correlations when both the coupling and temperature are increased. Additionally, evidence from other studies[41–43] suggests that non-Markovian environments are capable of sustaining quantum coherence. The interplay of these factors finally results in the increase of non-Markovianity with both temperature and coupling strength that we see in our results.

Results

The spin-boson model. The spin-boson model[1] is one of the most extensively studied models of open quantum systems, and is the one we employ here. It describes a spinor-like two-state system interacting with a bosonic environment. First, let us consider this standard model, which can be divided into three components

$$\hat{H}_{\mathrm{tot}} = \hat{H}_{\mathrm{sys}} + \hat{H}_{\mathrm{env}} + \hat{H}_{\mathrm{int}}. \tag{1}$$

The system Hamiltonian, $\hat{H}_{\mathrm{sys}}$, is written as

$$\hat{H}_{\mathrm{sys}} = \frac{\hbar\omega_0}{2}\hat{\sigma}_z + J\hat{\sigma}_x, \tag{2}$$

where $J\hat{\sigma}_x$ is the coherent-coupling term, which enables the tunneling between the two system quantum states, labeled as $|1\rangle$ and $|-1\rangle$, with the energy level spacing $\hbar\omega_0$. Usually, one adopts the delocalized basis $|\chi_+\rangle$ and $|\chi_-\rangle$ (exciton), which is defined by the following eigenvalue problem

$$\left(\frac{\hbar\omega_0}{2}\hat{\sigma}_z + J\hat{\sigma}_x\right)|\chi_\pm\rangle = \pm\frac{\hbar}{2}\Omega|\chi_\pm\rangle, \tag{3}$$

with $\Omega = \sqrt{\omega_0^2 + 4J^2/\hbar^2}$.

The environment, $\hat{H}_{\mathrm{env}}$, is usually modelled as a large collection of harmonic oscillators

$$\hat{H}_{\mathrm{env}} = \sum_{\mathbf{k}}\hbar\omega_{\mathbf{k}}\hat{a}_{\mathbf{k}}^\dagger\hat{a}_{\mathbf{k}}, \tag{4}$$

where $\hat{a}_{\mathbf{k}}^\dagger$ ($\hat{a}_{\mathbf{k}}$) is the creation (annihilation) operator of the environment mode $\mathbf{k}$ with angular frequency $\omega_{\mathbf{k}}$. For simplicity, a linear system-environment coupling, $\hat{H}_{\mathrm{int}}$, is adopted throughout this work:

$$\hat{H}_{\mathrm{int}} = \sum_{\mathbf{k}}\hat{\sigma}_z \otimes \left(\hbar g_{\mathbf{k}}\hat{a}_{\mathbf{k}}^\dagger + \hbar g_{\mathbf{k}}^*\hat{a}_{\mathbf{k}}\right), \tag{5}$$

where $g_{\mathbf{k}}$ is the coupling constant between the environment mode $\mathbf{k}$ and the system. In most physical problems, the details of the microscopic description of g_k are not clear, and one usually employs a spectral density function, $J(\omega)=\Sigma_{\mathbf{k}}|g_{\mathbf{k}}|^2\delta(\omega-\omega_{\mathbf{k}})$, to characterize the coupling strength via the reorganization energy $\lambda=\int_0^\infty J(\omega)/\omega d\omega$. The physical meaning of the spectral density function can be understood as the density of states of the environment, weighted by the coupling strengths. Moreover the way in which the environment modulates the dynamics of the system is described by the correlation function

$$G(t)=\int_0^\infty J(\omega)\left[\coth\left(\frac{\hbar\omega}{2k_BT}\right)\cos\ \omega t-i\ \sin\ \omega t\right]d\omega. \tag{6}$$

The real part is related to the dissipation process, while the imaginary part corresponds to the response function.

The statistical properties of the entire system can be described by the total density matrix ρ_{tot}, which contains all the degrees of freedom of the system and environment. If the correlation between the system and environment is negligible, the Born approximation can be used and the total density matrix can be factorized into

$$\rho_{\text{tot}}(t)=\rho_{\text{sys}}(t)\otimes\rho_{\text{env}}, \tag{7}$$

where $\rho_{\text{sys}}(t)$ describes the dynamics of the system and $\rho_{\text{env}}=\exp[-\hat{H}_{\text{env}}/k_BT]/Z$ is the environment density matrix in thermal equilibrium at temperature T. Here, k_B is the Boltzmann constant and $Z=\text{Tr}\ \exp[-\hat{H}_{\text{env}}/k_BT]$ is the partition function.

One notes that when ω_0, J, and λ are comparable, this makes the conventional perturbative treatment unreliable. In the following, we will adopt the two frequently-used perturbative but non-Markovian QME formalisms discussed in the introduction and compare their results with the exact one in the intermediate-coupling regime, as they both begin to break down, and investigate ways in which to evaluate their accuracy.

Second-order time-convolution equation (TC2). For the Hamiltonian defined above, the time evolution of the system density matrix $\rho_{\text{tot}}(t)$ under the TC2 approximation is expressed as

$$\frac{\partial}{\partial t}\rho_{\text{sys}}(t)=-\frac{1}{\hbar^2}\text{Tr}_{\text{env}}\times\int_0^t\left[\widetilde{H}_{\text{int}}(t),\left[\widetilde{H}_{\text{int}}(\tau),\rho_{\text{sys}}(\tau)\otimes\rho_{\text{env}}\right]\right]d\tau. \tag{8}$$

The tilde symbol above an operator denotes the interaction picture with respect to $\hat{H}_{\text{sys}}+\hat{H}_{\text{env}}$. The interaction Hamiltonian in terms of the delocalized basis can be expressed as

$$\widetilde{H}_{\text{int}}(t)=\sum_{\mu,\nu,\mathbf{k}}A_{\mu,\nu}e^{i\omega_{\mu,\nu}t}|\mu\rangle\langle\nu|\otimes\left(\hbar g_{\mathbf{k}}\hat{a}_{\mathbf{k}}^\dagger e^{i\omega_{\mathbf{k}}t}+\hbar g_{\mathbf{k}}^*\hat{a}_{\mathbf{k}}e^{-i\omega_{\mathbf{k}}t}\right), \tag{9}$$

where $A_{\mu,\nu}=\langle\mu|\hat{\sigma}_z|\nu\rangle$, and $\mu,\nu=\chi_+,\chi_-$. Substituting Eq. (9) into (8) with the explicit expansion leads to a set of simultaneous integrodifferential equations of the density matrix elements $\rho_{\mu,\nu}(t)$

$$\frac{\partial}{\partial t}\left[e^{-i\omega_{\alpha,\beta}t}\rho_{\alpha,\beta}(t)\right]=-i\omega_{\alpha,\beta}e^{-i\omega_{\alpha,\beta}t}\rho_{\alpha,\beta}(t)+\sum_{\mu,\nu}\int_0^t f_{\mu,\nu}(t-\tau)e^{-i\omega_{\mu,\nu}\tau}\rho_{\mu,\nu}(\tau)\,d\tau. \tag{10}$$

One notes that the memory effects are taken into account in terms of the convolution of the memory kernel $f_{\mu,\nu}(t-\tau)$. A detailed expression for this kernel is given in the Appendix.

To solve the simultaneous integrodifferential components of Eq. (10), we invoke the Laplace transformation $\mathcal{L}\{f\}:=\int_0^\infty f(t)e^{-st}dt$, and transform them into a set of algebraic equations. After carefully analyzing the properties of the poles, the conventional residual theorem enables one to accomplish the inverse Laplace transformation and move back from Laplace space into the time-domain.

Second-order time-local equation (TL2). In the TL2 formalism, the system is considered to be sluggish, hence the bath feedback on the system dynamics can be neglected by approximating $\rho_{\text{sys}}(t-\tau)\approx\exp\left[i\hat{H}_{\text{sys}}\tau/\hbar\right]\rho_{\text{sys}}(t)\exp\left[-i\hat{H}_{\text{sys}}\tau/\hbar\right]$. This assumption is reasonable because it is impossible for a system to change its configuration instantaneously. Consequently the system density matrix should be pulled out from the integral to obtain the following QME

$$\frac{\partial}{\partial t}\rho_{\text{sys}}(t)=-\frac{1}{\hbar^2}\text{Tr}_{\text{env}}\times\int_0^t\left[\widetilde{H}_{\text{int}}(t),\left[\widetilde{H}_{\text{int}}(\tau),\rho_{\text{sys}}(t)\otimes\rho_{\text{env}}\right]\right]d\tau. \tag{11}$$

Similarly, substituting Eq. (9) into (11) with the explicit expansion leads to a set of simultaneous differential equations of the density matrix elements $\rho_{\mu,\nu}(t)$

$$\frac{\partial}{\partial t}\left[e^{-i\omega_{\alpha,\beta}t}\rho_{\alpha,\beta}(t)\right] = -i\omega_{\alpha,\beta}e^{-i\omega_{\alpha,\beta}t}\rho_{\alpha,\beta}(t) + \sum_{\mu,\nu}\left(\int_0^t h_{\mu,\nu}(t-\tau)\,d\tau\right)e^{-i\omega_{\mu,\nu}t}\rho_{\mu,\nu}(t). \tag{12}$$

The detailed expression of the memory kernel $h_{\mu,\nu}(t-\tau)$ is given in the Appendix. It should be emphasized that although $\rho_{\mu,\nu}(t)$ is pulled out from the integral, Eq. (12) is capable of predicting a non-Markovian dynamics because the time integral of $h_{\mu,\nu}(t)$ results in time-varying coefficients in front of $\rho_{\mu,\nu}(t)$. Whether or not such differential equations behave non-Markovianly crucially depends on these time-varying coefficients.

Comparisons with exact results. To illustrate the differences of the approximations explicitly, we apply these two QMEs to a photosynthetic dimer model, which has attracted considerable interest recently[8,9,44–50]. We employ the Drude-Lorentz spectral density function (the over-damped Brownian oscillator model)[15,51], $J(\omega) = (2\lambda\gamma/\pi)[\omega/(\omega^2+\gamma^2)]$, which has been widely used for a range of theoretical studies of this type of system[46–50]. We use it here because it is convenient for the comparison with the HEOM. However, in reality, the spectral densities found in real photosynthetic systems tend to be much more complex[46], and while the HEOM can be extended to model such environments it typically involves a substantial additional numerical overhead[52]. As mentioned in the previous section, within the Drude-Lorentz spectral density the reorganization energy, λ, characterizes the coupling strength to the environment, while the quantity γ determines the width of the spectral density. These two parameters have considerable influence on the dynamics of the system.

In Fig. 1, we show the system dynamics given by (a) TC2, (b) HEOM, and (c) TL2 with varying λ and temperature T. The other parameters are fixed at $\omega_0 = 70\,\mathrm{cm}^{-1}$, $J = 100\,\mathrm{cm}^{-1}$, and $\gamma = 50\,\mathrm{cm}^{-1}$ ($\gamma^{-1} = 106\,\mathrm{fs}$). These parameters are typical in photosynthetic systems. The solid curves in each panel denote the populations of the $|\chi_+\rangle$ state with temperatures $T = 300\,\mathrm{K}$ (black), 250 K (red), and 200 K (blue), respectively. It can be seen that, at higher temperatures, the population of the $|\chi_+\rangle$ state transfers to the $|\chi_-\rangle$ state faster than at lower temperatures, but there is always a crossing so that the thermal equilibrium population of the $|\chi_+\rangle$ state is larger at higher temperatures.

For small values of λ, the results of the two QME models show excellent agreement with that of the HEOM, indicating that both TC2 and TL2 perform well in the weak system-environment coupling regime and that the bath memory effect is insignificant at small λ. Moreover, the result of TC2 completely coincides with that of the HEOM for very small couplings. We show the comparison between TC2 (solid curve) and HEOM (dot-dashed curve) methods in the inset of Fig. 1(a) for $\lambda = 5\,\mathrm{cm}^{-1}$, and $T = 250\,\mathrm{K}$. This is in line with a recent comparative work in Ref. 53. When λ is increased, the TC2 population results exhibit vigorous beating and produce oscillatory curves up to 800 fs, which is absent in the HEOM result. We attribute these oscillations to the over-estimation of the coherence by TC2. Apart from these beatings, the overall magnitude of the population of HEOM is quantitatively better approximated by TC2 than TL2. The TL2 model yields monotonically-decaying population dynamics that tends to reach thermal equilibrium too rapidly. This leads to a significant over-estimation of the population relaxation rate by TL2, especially at large λ. This over-estimation of the population relaxation rate in Redfield theory has been reported previously[54], and here we gain further insight into its origin by comparing to the TC2 results.

The dashed curves in Fig. 1 denote the absolute value of the off-diagonal elements of the system density matrix, i.e., the coherence between the $|\chi_+\rangle$ and $|\chi_-\rangle$ states. The results from the TC2 method manifestly show the over-estimation of the coherence even if λ is small. When λ is increased, the over-estimation of the coherence becomes quite pronounced. On the other hand, the coherence in the TL2 model decays more rapidly, leading to the sluggish dynamics discussed above. In summary, the coherence dynamics is better approximated by TL2, and the TC2 model may fail in approximating the true coherence for large λ. However, the overall population decay rate predicted by the TC2 is generally more correct than that of TL2. It is interesting to note that the TL2 model yields an exact QME for a pure dephasing spin-boson model (i.e. $J = 0$)[28] while the TC2 model underestimates the pure dephasing rate, which is in line with our findings here.

Benchmark of approximative QMEs. In the previous section, we analyzed how the coherence terms of the two approximations are qualitatively different from the HEOM exact results. However, those comparisons fail in providing an overall intuitive picture about which model performs better as they are basis-dependent. In other words, it is possible that one model may perform better or worse than another depending on the bases used. In this section, we apply a measure of the non-Markovianity to develop a bases-free benchmark which can quantitatively describe the performance of the approximate methods.

Entanglement and non-Markovianity. Let us consider an isolated ancilla possessing the same degrees of freedom of the system and with which the system forms a maximally entangled initial state $|\Psi\rangle = \sum_{j=\chi_+,\chi_-}\frac{1}{\sqrt{2}}|j\rangle \otimes |j\rangle$ (see Fig. 2). If the system evolves according to a process $\mathcal{E}_{t,0}$, then the Choi-Jamiołkowski isomorphism[39,40] guarantees that the extended density matrix

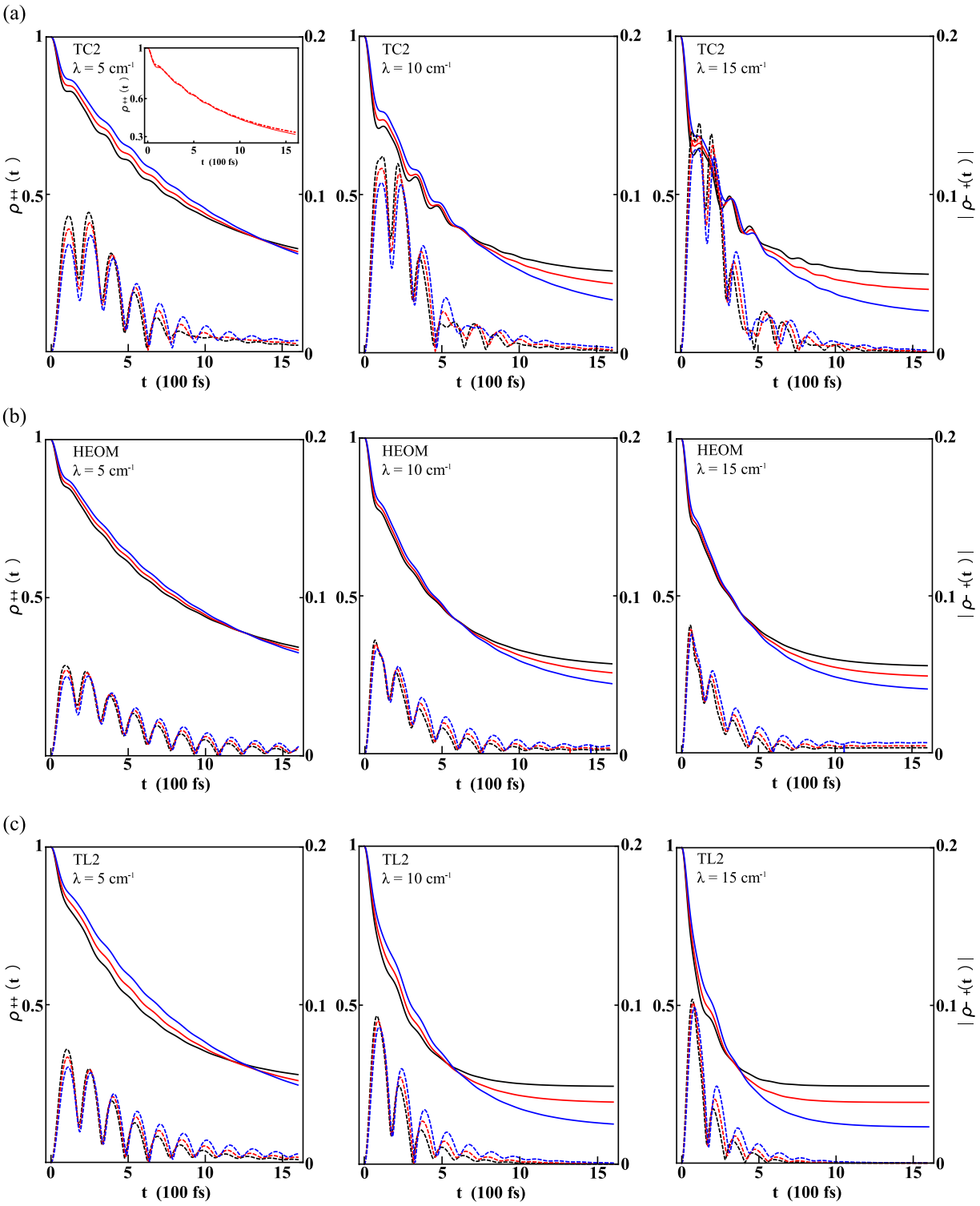

Figure 1. Comparisons between the dynamics given by threes models. Time evolution of the populations $\rho_{++}(t)$ (solid) and coherence $|\rho_{-+}(t)|$ (dashed) predicted by (**a**) TC2, (**b**) HEOM, and (**c**) TL2 for the spin-boson model with different values of λ at temperatures $T = 300\,\mathrm{K}$ (black), 250 K (red) and 200 K (blue). The other parameters are $\omega_0 = 70\,\mathrm{cm}^{-1}$, $J = 100\,\mathrm{cm}^{-1}$, and $\gamma = 50\,\mathrm{cm}^{-1}$ ($\gamma^{-1} = 106\,\mathrm{fs}$). For small λ, both QMEs yield excellent results, as expected. The inset in (**a**) shows the results given by TC2 (solid curve) and HEOM(dot-dashed curve) for $\lambda = 5\,\mathrm{cm}^{-1}$, and $T = 250\,\mathrm{K}$, illustrating how they almost overlap. However, due to over-estimation of the coherence, the result calculated from the TC2 method shows a slightly higher beating behavior in the population dynamics. In contrast, for large λ the population dynamics predicted by the TC2 method is in better agreement with those of the HEOM, whereas the populations given by the TL2 method are somewhat sluggish and tend to approach thermal equilibrium a bit faster.

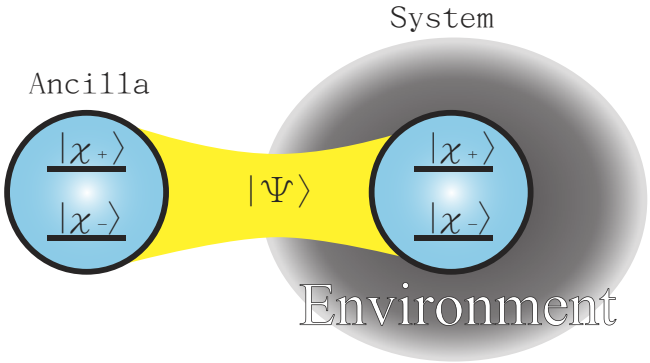

Figure 2. Schematic illustration of the entanglement measure. We consider a system and a copy of it acting as a well-isolated ancilla possessing the same degrees of freedom of the system. Initially, they form a maximally-entangled state $\rho_{\mathrm{sys,anc}}(0) = |\Psi\rangle\langle\Psi|$. Then the system starts to feel contact with its environment (denoted by the gray shadow) and evolves according to $\mathcal{E}_{t,0}$, whereas the ancilla is kept isolated.

$$\begin{aligned}\rho_{\mathrm{sys,anc}}(t) &= (\mathcal{E}_{t,0}\otimes\mathcal{I}_{\mathrm{anc}})(|\Psi\rangle\langle\Psi|)\\ &= \sum_{j,k}\frac{1}{2}\mathcal{E}_{t,0}(|j\rangle\langle k|)\otimes|j\rangle\langle k|.\end{aligned} \tag{13}$$

contains all the necessary information on the dynamics of the system, where $\mathcal{I}_{\mathrm{anc}}$ is the identity process acting on the ancilla. The entanglement, $\mathbf{E}(\rho_{\mathrm{sys,anc}})$, between the system and the ancilla is a physical quantity which is typically very sensitive to environmental effects.

Another related quantity is the degree of non-Markovianity, $\mathcal{NM}$. Recently, many efforts have been devoted to construct a proper measure of the non-Markovianity[32,33]. Rivas *et al.*[33] combine the concept of the divisibility of a quantum process[55,56] and the fact that no local completely positive (CP) operation[40] can increase the entanglement $\boldsymbol{E}$ between a system and its corresponding ancilla

$$\mathbf{E}\left[\rho_{\mathrm{sys,anc}}\right] \geq \mathbf{E}\left[\left(\mathcal{E}_{\mathrm{sys}}\otimes\mathcal{I}_{\mathrm{anc}}\right)\left(\rho_{\mathrm{sys,anc}}\right)\right]. \tag{14}$$

Consequently, Rivas *et al.*[33] proposed that the degree of non-Markovianity within a given time interval $[0, t]$ can be estimated by

$$\mathcal{NM} = \int_0^t \left|\frac{d}{d\tau}\mathbf{E}[(\mathcal{E}_{\tau,0}\otimes\mathcal{I}_{\mathrm{anc}})(|\Psi\rangle\langle\Psi|)]\right| d\tau - \Delta\mathbf{E}_t, \tag{15}$$

where

$$\Delta\mathbf{E}_t = \mathbf{E}[|\Psi\rangle\langle\Psi|] - \mathbf{E}[(\mathcal{E}_{t,0}\otimes\mathcal{I}_{\mathrm{anc}})(|\Psi\rangle\langle\Psi|)]. \tag{16}$$

The non-Markovianity of open-system quantum dynamics can be evaluated at many different theoretical levels[32–36], and the quantity $\mathcal{NM}$ is an extremely strict indicator of non-Markovianity that measures the information exchange in time between the system and its environment. For $\mathcal{NM}$ to have a non-zero value, explicit environmental memory effects must be present.

Here we compare the time evolution of the entanglement, $\boldsymbol{E}_t$, and the corresponding degree of non-Markovianity, $\mathcal{NM}$, for the two approximate system-bath models and show how they can provide an integrated picture as to what extent their dynamics deviate from the exact results.

Evaluating non-Markovianity. To analyse the behavior of the non-Markovianity in each method, in this section we will show how the concurrence, a well-known measure for bipartite entanglement[57], between system and ancilla evolves in time and how the corresponding non-Markovianity [Eq. (15)] depends on the physical parameters of the original spin-boson model.

As an explicit visualization of the integrand in Eq. (15), in Fig. 3, we apply the measure to (a) TC2, (b) HEOM, and (c) TL2 and show the time evolution of the concurrence for different values of λ at temperatures $T = 300\,\mathrm{K}$ (black), 250 K (red), and 200 K (blue), respectively. The other parameters are $\omega_0 = 70\,\mathrm{cm}^{-1}$, $J = 100\,\mathrm{cm}^{-1}$, and $\gamma = 50\,\mathrm{cm}^{-1}$ ($\gamma^{-1} = 106\,\mathrm{fs}$). It can be seen that, when increasing the temperature and λ, the decoherence becomes more pronounced. Hence, the concurrence will die out earlier for larger λ and higher temperature. As shown in Fig. 3(a), except for $\lambda = 5\,\mathrm{cm}^{-1}$, which produces monotonically-decreasing concurrence, the TC2 model produces oscillatory curves, in which

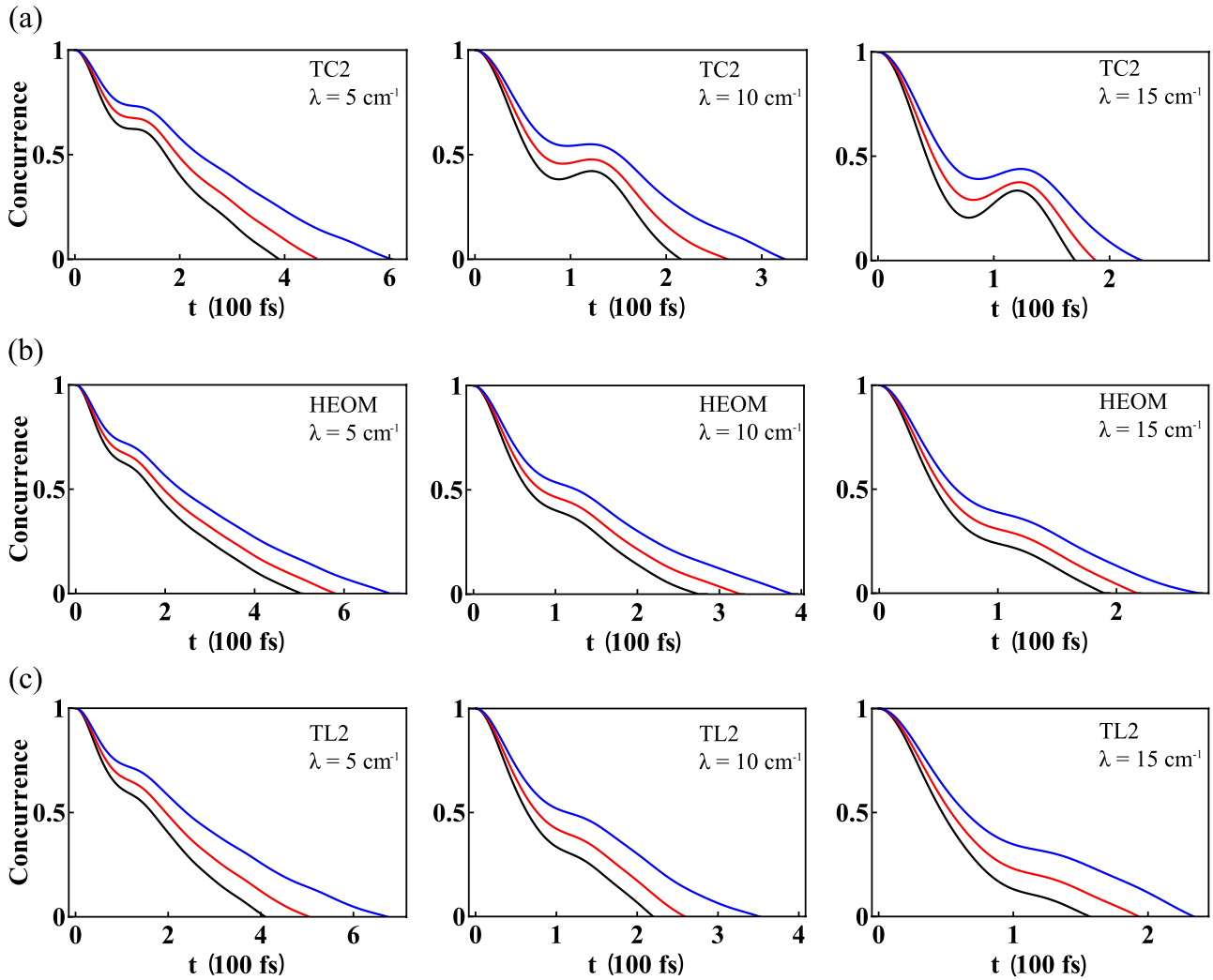

Figure 3. Time evolution of the concurrence given by threes models. Time evolution of the concurrence calculated by (**a**) TC2, (**b**) HEOM, and (**c**) TL2 for different values of λ at temperatures $T = 300\,\mathrm{K}$ (black), 250 K (red), and 200 K (blue). The other parameters are $\omega_0 = 70\,\mathrm{cm}^{-1}$, $J = 100\,\mathrm{cm}^{-1}$, and $\gamma = 50\,\mathrm{cm}^{-1}$ ($\gamma^{-1} = 106\,\mathrm{fs}$). In general, the concurrence will die out faster for larger λ and higher temperatures. The coherence over-estimation of the TC2 method is manifested by a concurrence revival around 100 fs for larger values of λ, whereas HEOM and TL2 produce a monotonically-decreasing concurrence.

a concurrence revival is exhibited around 100 fs and results in a finite degree of non-Markovianity (shown later). A similar entanglement revival can also be seen in biomolecular systems[58]. While in Fig. 3(b,c), HEOM and TL2 produce monotonically-decreasing concurrence and generate no visible non-Markovianity with this measure.

In Fig. 4, we show the corresponding measure of the non-Markovianity, $\mathcal{NM}$, calculated using the time evolution of the concurrence shown in Fig. 3(a). Only TC2, for larger λ values, leads to non-zero non-Markovianity, while TC2 at $\lambda = 5\,\mathrm{cm}^{-1}$, HEOM, and TL2 generate null results due to the monotonically-decreasing concurrence. This comparison not only shows that the TL2 yields a better approximation to the HEOM dynamics, but also explicitly demonstrates the degree to which TC2 deviates from HEOM. We again attribute this deviation to the over-estimation of coherence shown in Fig. 1. In addition, it can be seen in Fig. 4 that $\mathcal{NM}$ tends to increase with increasing λ and temperature. We will investigate this below in a regime where the HEOM results exhibit similar behavior.

Increase of non-Markovianity with λ and temperature. The other two important parameters in our spin-boson model are the level spacing ω_0 and the bath relaxation time γ. The former affects to what extent the state $|\chi_+\rangle$ is delocalized, while the latter is related to the correlation time of the environment and is directly connected to the non-Markovianity of the system.

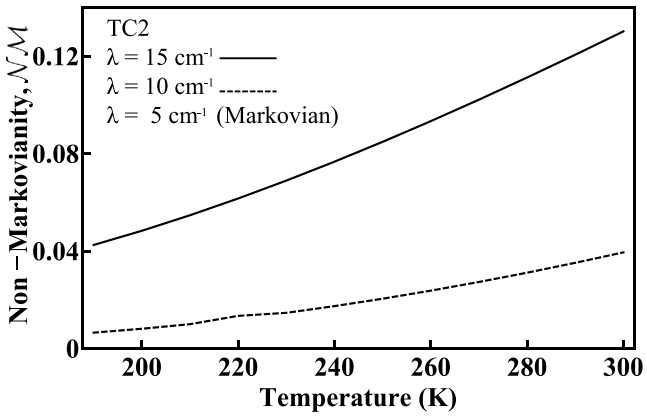

Figure 4. Non-Markovianity, $\mathcal{NM}$, obtained by the TC2 method as a function of temperature. The parameters are the same as used in Fig. 3. Among the three methods investigated in this work, only TC2 at higher λ generates non-zero non-Markovianity for these parameters. At $\lambda = 5\,\mathrm{cm}^{-1}$ TC2 correctly produces the expected Markovian dynamics for this regime.

In Fig. 5(a), we reduce ω_0 to $40\,\mathrm{cm}^{-1}$ and fix the other parameters at $\lambda = 5\,\mathrm{cm}^{-1}$, $\gamma = 50\,\mathrm{cm}^{-1}$, and $T = 200\,\mathrm{K}$. The reduction of ω_0 leads to a manifest concurrence revival around 100 fs in the TC2 concurrence dynamics, a result of stronger delocalization and significant enhancement of the coherence effect. An analogous result can be seen in Ref. 37. In the mean time, the concurrence of the HEOM result is still monotonically decreasing. The TC2 model further over-estimates this enhancement and ends up with finite non-Markovianity within all range of temperatures shown in Fig. 5(b). The TL2 model predicts almost-Markovian results, besides the very small non-Markovianity at low temperatures, again showing a better agreement with the HEOM exact results.

In Fig. 6(a), γ is further reduced to $20\,\mathrm{cm}^{-1}$ ($\gamma^{-1} = 265\,\mathrm{fs}$) to investigate the effect of slow environments. As the spectral density function is narrower, the correlation time of the environment becomes long compared with the characteristic time of the system dynamics. Hence the information on the system dynamics is more likely to be retained in the environment and flow back into the system. This back-flow of information in turn affects the behavior of the system and results in beating in the concurrence curves for all methods. As shown in Fig. 6(b), the TC2 model predicts a non-Markovianity much larger than the exact results. On the other hand, the TL2 model predicts a non-Markovianity in excellent agreement with the HEOM results, with only a small under-estimation of the non-Markovianity in this set of parameters.

The above comparisons exhibit an interesting tendency for $\mathcal{NM}$ to increase with λ and temperature. Several relevant theoretical and experimental works have reported[41–43] that strong system-environment correlations are helpful for maintaining quantum coherence even at high temperatures. As a result, higher temperature may in turn activate more phonon modes in the environment without destroying the quantum coherence significantly. This provides more channels via which the system can interact with the environment. In the language of quantum information science, smaller γ and strong system-environment correlation may help to preserve the dynamical information; while larger λ and higher temperature may increase the possibility that this information can flow back into the system from the environment. Consequently, this increase of $\mathcal{NM}$ with larger temperature and λ is a result of the competition between the back-flow of information and thermal fluctuations. Meanwhile, the magnitude of the concurrence is reduced by the stronger random fluctuations in the environment.

Discussion

In summary, we first investigate the dynamics of two perturbative second-order QME methods, TC2 and TL2, and compare their results with the numerically-exact results calculated by HEOM. We find that TC2 can approximate the HEOM population better than TL2. However, a drawback of the TC2 model is its over-estimation of the coherence. This drawback results in the TC2 model predicting too much beating behavior in the population dynamics and limits the accuracy of TC2. In constrast, the TL2 model predicts sluggish dynamics and loss of coherence faster than that of the exact HEOM. As a result, the population tends to reach thermal equilibrium too rapidly.

To further investigate the dynamics and establish a benchmark for the performance of perturbative QMEs, we combine the concept of Choi-Jamiokowski isomorphism[39,40], entanglement with an ancilla[57], and a measure of non-Markovianity[33] to provide a quantitative way to determine how much the coherence dynamics and memory effects are deviating from the exact result. This provides a deep physical insight on the effects of each parameter and a single quantity to determine how much the QME dynamics deviates from the exact results. Here we find that the non-Markovian measure indicates that the TL2 approximates HEOM better than TC2 in terms of the coherence dynamics and memory effects for the

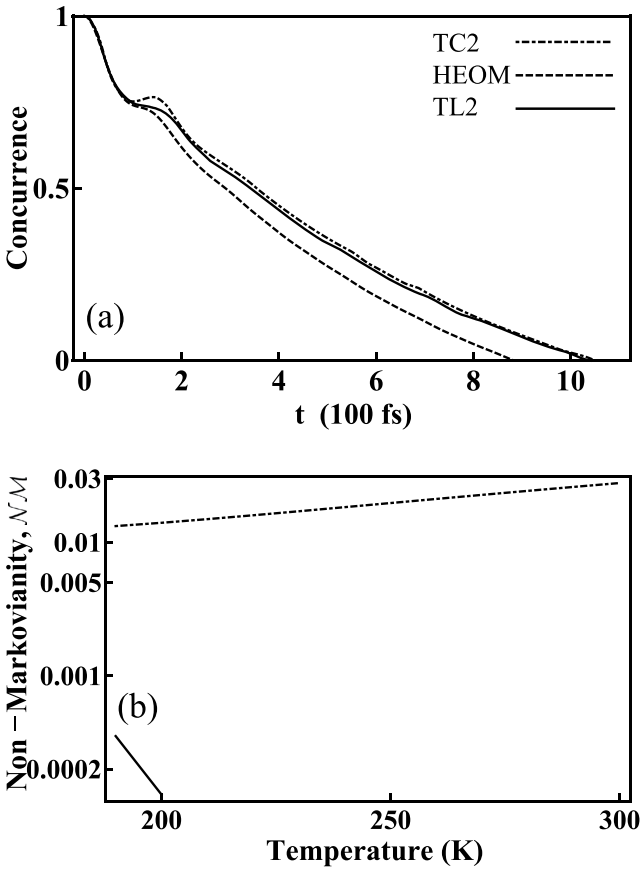

Figure 5. The effects of reduction of ω_0. (**a**) The concurrence obtained from the TC2 method (dot-dashed), HEOM (dashed), and TL2 (solid), for $\omega_0 = 40\,\mathrm{cm}^{-1}$. The reduction of ω_0 leads to a manifest concurrence revival around 100 fs. The concurrence obtained from HEOM is still monotonically decreasing. The other parameters are: $\lambda = 5\,\mathrm{cm}^{-1}$, $\gamma = 50\,\mathrm{cm}^{-1}$, and $T = 200$ K. (**b**) The corresponding non-Markovianity versus temperature. The result of TC2 shows finite non-Markovianity, while that from TL2 shows very small non-Markovianity and only at low temperatures. The result from HEOM is Markovian due to its monotonically-decreasing concurrence.

dimer system studied here. In addition, while it is well understood that the reorganization energy λ and temperature enhance the effect of thermal fluctuations in the environment on the system, increasing these parameters can have surprising results. In particular, our results show that higher temperature increases information back-flow from the environment, thus increasing the non-Markovianity of the system dynamics, even though the concurrence itself undergoes faster decay. Note that photosynthetic systems and other molecular light-harvesting networks are in general far more complex than the models studied here[4,5], and more general models should be considered for realistic systems[59–62]. Nevertheless, the focus of this work is the physics revealed in the comparison of the theoretical methods and the application of the non-Markovianity measure for revealing new physical insights. The theoretical methods examined here have often been applied to model real photosynthetic systems, and the quantitative measures we employ are themselves model independent. The non-Markovianity analysis proposed here could be easily used to investigate coherence dynamics in more complex systems and more general models. Therefore, these results could have important implications in the theoretical modeling of electronic coherence in photosynthetic systems[8,9,47].

Methods

Full expressions for the TC2 and TL2 quantum master equations. The detailed expression of the TC2 integrodifferential QMEs Eq. (10) is given by

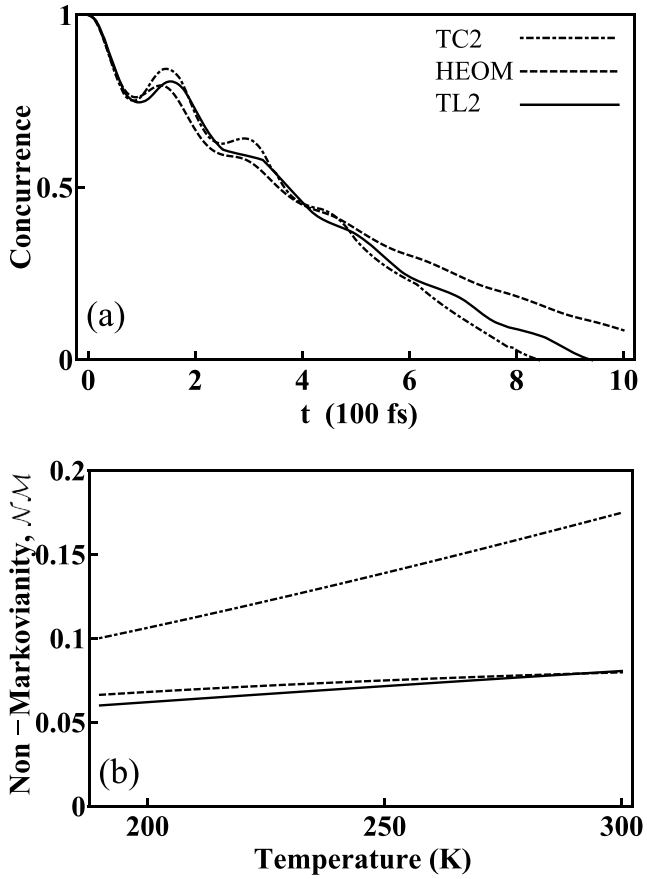

Figure 6. The effects of reduction of γ. (**a**) The concurrence versus time for TC2 (dot-dashed), HEOM (dashed), and TL2 (solid). The γ value is further reduced to 20 cm^{-1} ($\gamma^{-1} = 265$ fs). The other parameters are the same as those in Fig. 5(a). The information on the system dynamics can possibly flow back from the environment into the system and in turn leads to wavy concurrence curves. (**b**) The corresponding non-Markovianity values versus temperature. These non-Markovianity values increase prominently as a result of the reduced γ value. TC2 shows larger non-Markovianity values, while TL2 shows good agreement with the HEOM.

$$\begin{aligned}\frac{\partial}{\partial t}\left[e^{-i\omega_{\alpha,\beta}t}\rho_{\alpha,\beta}(t)\right] = & -i\omega_{\alpha,\beta}\exp[-i\omega_{\alpha,\beta}t]\rho_{\alpha,\beta}(t)\\ & + \sum_{\mu,\nu}A_{\alpha,\nu}A_{\mu,\beta}\int_0^t G(t-\tau)e^{i\omega_{\mu,\alpha}(t-\tau)}e^{-i\omega_{\nu,\mu}\tau}\rho_{\nu,\mu}(\tau)\,d\tau\\ & - \sum_{\mu,\nu}A_{\alpha,\nu}A_{\nu,\mu}\int_0^t\int_0^t G(t-\tau)e^{i\omega_{\beta,\nu}(t-\tau)}e^{-i\omega_{\mu,\beta}\tau}\rho_{\mu,\beta}(\tau)\,d\tau\\ & + \sum_{\mu,\nu}A_{\alpha,\nu}A_{\mu,\beta}\int_0^t G^*(t-\tau)e^{i\omega_{\beta,\nu}(t-\tau)}e^{-i\omega_{\nu,\mu}\tau}\rho_{\nu,\mu}(\tau)\,d\tau\\ & - \sum_{\mu,\nu}A_{\nu,\mu}A_{\mu,\beta}\int_0^t G^*(t-\tau)e^{i\omega_{\mu,\alpha}(t-\tau)}e^{-i\omega_{\alpha,\nu}\tau}\rho_{\alpha,\nu}(\tau)\,d\tau,\end{aligned} \tag{17}$$

where $G(t)$ is the correlation function defined by Eq. (6). Whereas the detailed expression of TL2 QME in Eq. (12) is given by

$$\begin{aligned}\frac{\partial}{\partial t}\left[e^{-i\omega_{\alpha,\beta}t}\rho_{\alpha,\beta}(t)\right] = & -i\omega_{\alpha,\beta}\exp\left[-i\omega_{\alpha,\beta}t\right]\rho_{\alpha,\beta}(t)\\ & +\sum_{\mu,\nu}A_{\alpha,\nu}A_{\mu,\beta}\int_0^t G(t-\tau)e^{i\omega_{\nu,\alpha}(t-\tau)}e^{-i\omega_{\nu,\mu}t}\rho_{\nu,\mu}(t)\,d\tau\\ & -\sum_{\mu,\nu}A_{\alpha,\nu}A_{\nu,\mu}\int_0^t G(t-\tau)e^{i\omega_{\mu,\nu}(t-\tau)}e^{-i\omega_{\mu,\beta}t}\rho_{\mu,\beta}(t)\,d\tau\\ & +\sum_{\mu,\nu}A_{\alpha,\nu}A_{\mu,\beta}\int_0^t G^*(t-\tau)e^{i\omega_{\beta,\mu}(t-\tau)}e^{-i\omega_{\nu,\mu}t}\rho_{\nu,\mu}(t)\,d\tau\\ & -\sum_{\mu,\nu}A_{\nu,\mu}A_{\mu,\beta}\int_0^t G^*(t-\tau)e^{i\omega_{\mu,\nu}(t-\tau)}e^{-i\omega_{\alpha,\nu}t}\rho_{\alpha,\nu}(t)\,d\tau. \end{aligned} \quad (18)$$

References

1. Leggett, A. J., Chakravarty, S., Dorsey, A. T., Fisher, M. P. A., Garg, A. & Zwerger, W. Dynamics of the dissipative two-state system. *Rev. Mod. Phys.* **59,** 1, doi: 10.1103/RevModPhys.59.1 (1987).
2. Weiss, U. *Quantum Dissipative Systems*, 4th ed. (World Scientific, Singapore, 2012).
3. Breuer, H.-P. & Petruccione, F. *The Theory of Open Quantum Systems* (Oxford University Press, New York, 2002).
4. van Amerongen, H., Valkunas, L. & van Grondelle, R. *Photosynthetic excitons* (World Scientific Pub Co Inc, 2000).
5. Burghardt, I., May, V., Micha, D. A. & Bittner, E. R. *Energy Transfer Dynamics in Biomaterial Systems* (Springer, 2009).
6. Layfield, J. P. & Hammes-Schiffer, S. Hydrogen tunneling in enzymes and biomimetic models. *Chem. Rev.* **114,** 3466, doi: 10.1021/cr400400p (2014).
7. Reece, S. Y. & Nocera, D. G. Proton-coupled electron transfer in biology: Results from synergistic studies in natural and model systems. *Annu. Rev. Biochem.* **78,** 673, doi: 10.1146/annurev.biochem.78.080207.092132 (2009).
8. Cheng, Y.-C. & Fleming, G. R. Dynamics of light harvesting in photosynthesis. *Annu. Rev. Phys. Chem.* **60,** 241, doi: 10.1146/annurev.physchem.040808.090259 (2009).
9. Lambert, N. *et al.* Quantum biology. *Nat. Phys.* **9,** 10, doi: 10.1038/nphys2474 (2013).
10. Grabert, H., Schramm, P. & Ingold, G.-L. Quantum brownian motion: The functional integral approach. *Phys. Rep.* **168,** 115, doi: 10.1016/0370-1573(88)90023-3 (1988).
11. Grifoni, M. & Hänggi, P. Driven quantum tunneling. *Phys. Rep.* **304,** 229, doi: 10.1016/S0370-1573(98)00022-2 (1998).
12. Egger, R., Mühlbacher, L. & Mak, C. H. Path-integral monte carlo simulations without the sign problem: Multilevel blocking approach for effective actions. *Phys. Rev. E* **61,** 5961, doi: 10.1103/PhysRevE.61.5961 (2000).
13. Tanimura, Y. Nonperturbative expansion method for a quantum system coupled to a harmonic-oscillator bath. *Phys. Rev. A* **41,** 6676, doi: 10.1103/PhysRevA.41.6676 (1990).
14. Tanimura, Y. & Kubo, R. Time evolution of a quantum system in contact with a nearly gaussian-markoffian noise bath. *J. Phys. Soc. Jpn.* **58,** 101, doi: 10.1143/JPSJ.58.101 (1989).
15. Tanimura, Y. Stochastic liouville, langevin, fokker-planck, and master equation approaches to quantum dissipative systems. *J. Phys. Soc. Jpn.* **75,** 082001, doi: 10.1143/JPSJ.75.082001 (2006).
16. Xu, R.-X. & Yan, Y. Dynamics of quantum dissipation systems interacting with bosonic canonical bath: Hierarchical equations of motion approach. *Phys. Rev. E* **75,** 031107, doi: 10.1103/PhysRevE.75.031107 (2007).
17. Iles-Smith, J., Lambert, N. & Nazir, A. Environmental dynamics, correlations, and the emergence of noncanonical equilibrium states in open quantum systems. *Phys. Rev. A* **90,** 032114, doi: 10.1103/PhysRevA.90.032114 (2014).
18. Garg, A., Onuchic, J. N. & Ambegaokar, V. Effect of friction on electron transfer in biomolecules. *J. Chem. Phys.* **83,** 4491, doi: 10.1063/1.449017 (1985).
19. Redfield, A. G. The theory of relaxation processes. *Advan. Magn. Reson.* **1,** 1, doi: 10.1016/B978-1-4832-3114-3.50007-6 (1965).
20. Förster, T. Energiewanderung und fluoreszenz. *Naturwiss.* **33,** 166, doi: 10.1007/BF00585226 (1946).
21. Förster, T. Zwischenmolekulare energiewanderung und fluoreszenz. *Ann. der Phys.* **437,** 55, doi: 10.1002/andp.19484370105 (1948).
22. Förster, T. Transfer mechanisms of electronic excitation energy. *Radiat. Res. Suppl.* **2,** 326, doi: 10.2307/3583604 (1960).
23. Hänggi, P., Talkner, P. & Borkovec, M. Reaction-rate theory: fifty years after kramers. *Rev. Mod. Phys.* **62,** 251, doi: 10.1103/RevModPhys.62.251 (1990).
24. Shibata, F. & Arimitsu, T. Expansion formulas in nonequilibrium statistical mechanics. *J. Phys. Soc. Jpn.* **49,** 891, doi: 10.1143/JPSJ.49.891 (1980).
25. Mukamel, S., Oppenheim, I. & Ross, J. Statistical reduction for strongly driven simple quantum systems. *Phys. Rev. A* **17,** 1988, doi: 10.1103/PhysRevA.17.1988 (1978).
26. Meier, C. & Tannor, D. J. Non-markovian evolution of the density operator in the presence of strong laser fields. *J. Chem. Phys.* **111,** 3365, doi: 10.1063/1.479669 (1999).
27. Kleinekathöfer, U. Non-markovian theories based on a decomposition of the spectral density. *J. Chem. Phys.* **121,** 2505, doi: 10.1063/1.1770619 (2004).
28. Palenberg, M. A., Silbey, R. J., Warns, C. & Reineker, P. Local and nonlocal approximation for a simple quantum system. *J. Chem. Phys.* **114,** 4386, doi: 10.1063/1.1330213 (2001).
29. Jin, J., Zheng, X. & Yan, Y. Exact dynamics of dissipative electronic systems and quantum transport: Hierarchical equations of motion approach. *J. Chem. Phys.* **128,** 234703, doi: 10.1063/1.2938087 (2008).
30. Strümpfer, J. & Schulten, K. Open quantum dynamics calculations with the hierarchy equations of motion on parallel computers. *J. Chem. Theory Comput.* **8,** 2808, doi: 10.1021/ct3003833 (2012).
31. Liu, H., Zhu, L., Bai, S. & Shi, Q. Reduced quantum dynamics with arbitrary bath spectral densities: Hierarchical equations of motion based on several different bath decomposition schemes. *J. Chem. Phys.* **140,** 134106, doi: 10.1063/1.4870035 (2014).
32. Breuer, H.-P., Laine, E.-M. & Piilo, J. Measure for the degree of non-markovian behavior of quantum processes in open systems. *Phys. Rev. Lett.* **103,** 210401, doi: 10.1103/PhysRevLett.103.210401 (2009).
33. Rivas, A., Huelga, S. F. & Plenio, M. B. Entanglement and non-markovianity of quantum evolutions. *Phys. Rev. Lett.* **105,** 050403, doi: 10.1103/PhysRevLett.105.050403 (2010).
34. Chruściński, D. & Maniscalco, S. Degree of non-markovianity of quantum evolution. *Phys. Rev. Lett.* **112,** 120404, doi: 10.1103/PhysRevLett.112.120404 (2014).

35. Bylicka, B., Chruściński, D. & Maniscalco, S. Non-markovianity and reservoir memory of quantum channels: a quantum information theory perspective. *Sci. Rep.* **4,** 5720, doi: 10.1038/srep05720 (2014).
36. Fanchini, F. F. *et al.* Non-markovianity through accessible information. *Phys. Rev. Lett.* **112,** 210402, doi: 10.1103/PhysRevLett.112.210402 (2014).
37. Mujica-Martinez, C. A., Nalbach, P. & Thorwart, M. Organic π-conjugated copolymers as molecular charge qubits. *Phys. Rev. Lett.* **111,** 016802, doi: 10.1103/PhysRevLett.111.016802 (2013).
38. Mujica-Martinez, C. A., Nalbach, P. & Thorwart, M. Quantification of non-markovian effects in the fenna-matthews-olson complex. *Phys. Rev. E* **88,** 062719, doi: 10.1103/PhysRevE.88.062719 (2013).
39. Jamiołkowski, A. Linear transformations which preserve trace and positive semidefiniteness of operators. *Rep. Math. Phys.* **3,** 275, doi: 10.1016/0034-4877(72)90011-0 (1972).
40. Choi, M.-D. Completely positive linear maps on complex matrices. *Linear Alg. Appl.* **10,** 285, doi: 10.1016/0024-3795(75)90075-0 (1975).
41. Nazir, A. Correlation-dependent coherent to incoherent transitions in resonant energy transfer dynamics. *Phys. Rev. Lett.* **103,** 146404, doi: 10.1103/PhysRevLett.103.146404 (2009).
42. Lee, H., Cheng, Y.-C. & Fleming, G. R. Coherence dynamics in photosynthesis: Protein protection of excitonic coherence. *Science* **316,** 1462, doi: 10.1126/science.1142188 (2007).
43. Collini, E. *et al.* Coherently wired light-harvesting in photosynthetic marine algae at ambient temperature. *Nature* **463,** 644, doi: 10.1038/nature08811 (2010).
44. Zigmantas, D. *et al.* Two-dimensional electronic spectroscopy of the b800-b820 light-harvesting complex. *Proc. Natl. Acad. Sci. USA* **103,** 12672, doi: 10.1073/pnas.0602961103 (2006).
45. Novoderezhkin, V. I. & van Grondelle, R. Physical origins and models of energy transfer in photosynthetic light-harvesting. *Phys. Chem. Chem. Phys.* **12,** 7352, doi: 10.1039/C003025B (2010).
46. Nalbach, P., Braun, D. & Thorwart, M. Exciton transfer dynamics and quantumness of energy transfer in the fenna-matthews-olson complex. *Phys. Rev. E* **84,** 041926, doi: 10.1103/PhysRevE.84.041926 (2011).
47. Pachon, L. A. & Brumer, P. Computational methodologies and physical insights into electronic energy transfer in photosynthetic light-harvesting complexes. *Phys. Chem. Chem. Phys.* **14,** 10094, doi: 10.1039/C2CP40815E (2012).
48. Ishizaki, A. & Fleming, G. R. Unified treatment of quantum coherent and incoherent hopping dynamics in electronic energy transfer: Reduced hierarchy equation approach. *J. Chem. Phys.* **130,** 234111, doi: 10.1063/1.3155372 (2009).
49. Ishizaki, A. & Fleming, G. R. Theoretical examination of quantum coherence in a photosynthetic system at physiological temperature. *Proc. Natl. Acad. Sci. USA* **106,** 17255, doi: 10.1073/pnas.0908989106 (2009).
50. Chen, H.-B., Lien, J.-Y., Hwang, C.-C. & Chen, Y.-N. Long-lived quantum coherence and non-markovianity of photosynthetic complexes. *Phys. Rev. E* **89,** 042147, doi: 10.1103/PhysRevE.89.042147 (2014).
51. Mukamel, S. *Principles of Nonlinear Optical Spectroscop* (Oxford University Press, New York, 1995).
52. Kreisbeck, C. & Kramer, T. Long-lived electronic coherence in dissipative exciton dynamics of light-harvesting complexes. *J. Phys. Chem. Lett.* **3,** 2828, doi: 10.1021/jz3012029 (2012).
53. Nalbach, P., Ishizaki, A., Fleming, G. R. & Thorwart, M. Iterative path-integral algorithm versus cumulant time-nonlocal master equation approach for dissipative biomolecular exciton transport. *New J. Phys.* **13,** 063040, doi: 10.1088/1367-2630/13/6/063040 (2011).
54. Ishizaki, A. & Fleming, G. R. On the adequacy of the redfield equation and related approaches to the study of quantum dynamics in electronic energy transfer. *J. Chem. Phys.* **130,** 234110, doi: 10.1063/1.3155214 (2009).
55. Wolf, M. & Cirac, J. Dividing quantum channels. *Comm. Math. Phys.* **279,** 147, doi: 10.1007/s00220-008-0411-y (2008).
56. Wolf, M. M., Eisert, J., Cubitt, T. S. & Cirac, J. I. Assessing non-markovian quantum dynamics. *Phys. Rev. Lett.* **101,** 150402, doi: 10.1103/PhysRevLett.101.150402 (2008).
57. Wootters, W. K. Entanglement of formation of an arbitrary state of two qubits. *Phys. Rev. Lett.* **80,** 2245, doi: 10.1103/PhysRevLett.80.2245 (1998).
58. Thorwart, M., Eckel, J., Reina, J., Nalbach, P. & Weiss, S. Enhanced quantum entanglement in the non-markovian dynamics of biomolecular excitons. *Chem. Phys. Lett.* **478,** 234, doi: 10.1016/j.cplett.2009.07.053 (2009).
59. Scholak, T., de Melo, F., Wellens, T., Mintert, F. & Buchleitner, A. Efficient and coherent excitation transfer across disordered molecular networks. *Phys. Rev. E* **83,** 021912, doi: 10.1103/PhysRevE.83.021912 (2011).
60. Alicki, R. & Miklaszewski, W. A resonance mechanism of efficient energy transfer mediated by fenna-matthews-olson complex. *J. Chem. Phys.* **136,** 134103, doi: 10.1063/1.3697975 (2012).
61. Walschaers, M., Diaz, J. F.-d.-C., Mulet, R. & Buchleitner, A. Optimally designed quantum transport across disordered networks. *Phys. Rev. Lett.* **111,** 180601, doi: 10.1103/PhysRevLett.111.180601 (2013).
62. Mostarda, S., Levi, F., Prada-Gracia, D., Mintert, F. & Rao, F. Structure-dynamics relationship in coherent transport through disordered systems. *Nat. Commun.* **4,** 2296, doi: 10.1038/ncomms3296 (2013).

Acknowledgements

This work is supported partially by the National Center for Theoretical Sciences and Minister of Science and Technology, Taiwan, grant numbers NSC 101-2628-M-006-003-MY3, and MOST 103-2112-M-006 -017 -MY4. FN is partially supported by the RIKEN iTHES Project, MURI Center for Dynamic Magneto-Optics, and a Grant-in-Aid for Scientific Research (S). YCC thanks the Ministry of Science and Technology, Taiwan (Grant No. NSC 100-2113-M-002-008-MY3).

Author Contributions

Y.C.C., Y.N.C. and F.N. designed this work. H.B.C. and N.L. carried out the calculations. All authors contributed to the discussions and the writing of the manuscript.

Additional Information

Competing financial interests: The authors declare no competing financial interests.

How to cite this article: Chen, H.-B. *et al.* Using non-Markovian measures to evaluate quantum master equations for photosynthesis. *Sci. Rep.* **5**, 12753; doi: 10.1038/srep12753 (2015).

This work is licensed under a Creative Commons Attribution 4.0 International License. The images or other third party material in this article are included in the article's Creative Commons license, unless indicated otherwise in the credit line; if the material is not included under the Creative Commons license, users will need to obtain permission from the license holder to reproduce the material. To view a copy of this license, visit http://creativecommons.org/licenses/by/4.0/